ELSEVIER

Toxicon 51 (2008) 334–344

TOXICON

www.elsevier.com/locate/toxicon

# Modulation of voltage-gated $Na^+$ and $K^+$ channels by pumiliotoxin **251D**: A "joint venture" alkaloid from arthropods and amphibians ☆

Thomas Vandendriessche[a], Yousra Abdel-Mottaleb[a], Chantal Maertens[a], Eva Cuypers[a], Alexander Sudau[b,1], Udo Nubbemeyer[b], Dietrich Mebs[c], Jan Tytgat[a,*]

[a]*Laboratory of Toxicology, University of Leuven, Leuven, Belgium*
[b]*Institute of Organic Chemistry, University of Mainz, Mainz, Germany*
[c]*Zentrum der Rechtsmedizin, University of Frankfurt, Frankfurt, Germany*

Received 6 August 2007; received in revised form 11 October 2007; accepted 12 October 2007
Available online 24 October 2007

## Abstract

Certain amphibians provide themselves with a chemical defense by accumulating lipophilic alkaloids into skin glands from dietary arthropods. Examples of such alkaloids are pumiliotoxins (PTXs). In general, PTXs are known as positive modulators of voltage-gated sodium channels (VGSCs). Unlike other PTXs, PTX **251D** does not share this characteristic. However, mice and insect studies showed that PTX **251D** is highly toxic and to date the basis of its toxicity remains unknown.

In this work, we searched for the possible target of PTX **251D**. The toxin was therefore made synthetically and tested on four VGSCs (mammalian $rNa_v1.2/\beta_1$, $rNa_v1.4/\beta_1$, $hNa_v1.5/\beta_1$ and insect *Para/tipE*) and five voltage-gated potassium channels (VGPCs) (mammalian $rK_v1.1$-$1.2$, $hK_v1.3$, $hK_v11.1$ (hERG) and insect *Shaker IR*) expressed heterologously in *Xenopus laevis* oocytes, using the two-electrode voltage clamp technique.

PTX **251D** not only inhibited the $Na^+$ influx through the mammalian VGSCs but also affected the steady-state activation and inactivation. Interestingly, in the insect ortholog, the inactivation process was dramatically affected. Additionally, PTX **251D** inhibited the $K^+$ efflux through all five tested VGPCs and slowed down the deactivation kinetics of the mammalian VGPCs. $hK_v1.3$ was the most sensitive channel, with an $IC_{50}$ value $10.8 \pm 0.5\,\mu M$. To the best of our knowledge this is the first report of a PTX affecting VGPCs.


*Keywords:* PTX **251D**; PTXs; VGSC; VGPC; Two-electrode voltage clamp technique

## 1. Introduction

A remarkable diversity of biologically active alkaloids has been discovered in amphibian skin (Daly et al., 2005). During evolution, certain amphibians have developed an efficient system to accumulate some of these toxic compounds from

☆*Ethical statement*: The authors declare that the article submitted for publication has not been published elsewhere and that the guidelines for animal welfare have been followed.

*Corresponding author.
*E-mail address:* Jan.Tytgat@pharm.kuleuven.be (J. Tytgat).
[1]Present address: ALTANA Pharma AG, Byk-Gulden-Street 2, Konstanz, Germany.

0041-0101/$ - see front matter © 2007 Elsevier Ltd. All rights reserved.
doi:10.1016/j.toxicon.2007.10.011

dietary alkaloid-containing arthropods into their skin. Together with the bright warning skin coloration, the accumulation of toxins offers an extreme evolutionary advantage against predators. Examples of such toxins are the lipophilic alkaloids pumiliotoxins (PTXs) that are very widely distributed in alkaloid-containing anurans from the neotropics (*Dendrobates*, *Epipedobates*, *Minyobates*, *Phylobates*, *Oophaga*, *Ameerga* and *Ranitomeya*), semi-temperate South America (*Melanophryniscus*), Madagascar (*Mantella*) and Australia (*Pseudophryne*). The presence of PTX **307A** and **323A** (Fig. 1) has also been reported in formicine ants of the genera *Brachymyrmex* and *Paratrechina* (Saporito et al., 2004). Recently, in the extracts of scheloribatid mites PTX **251D** (Fig. 1) was found together with PTX **237A** and 8-deoxyPTX **193H** (Takada et al., 2005), while PTXs **251D**, **307F** and **307A** and a homoPTX **251R** were found in oribatid mites from Costa Rica and Panama (Saporito et al., 2007). It has been proposed that mites are the major source of PTXs and other frog skin alkaloids with branches in their carbon skeletons.

PTXs are known to be toxic. They are described as potent cardiotonic agents with positive modulatory effects on voltage-gated sodium channels (VGSCs) (Daly et al., 1985). Like other PTXs, PTX **251D** is highly toxic, inducing convulsions and death to mice and insects ($LD_{50}$ being, respectively, 10 mg/kg and 150 ng/larvae) (Bargar et al., 1995; Daly et al., 2003). In addition, this toxin seems to repel predatory and ectoparasitic arthropods, and hence, its function in anuran chemical defense is proved (Weldon et al., 2006). However, earlier studies in brain synaptoneurosomes showed that PTX **251D** only weakly stimulates the sodium flux at low concentrations (10 μM) and has inhibitory effects on VGSCs at higher concentrations (100 μM) (Daly et al., 1985, 1990). Therefore, the observed effects in mice and insects cannot be explained by a modulation of VGSCs alone, making the possible physiological target(s) for this toxin unknown.

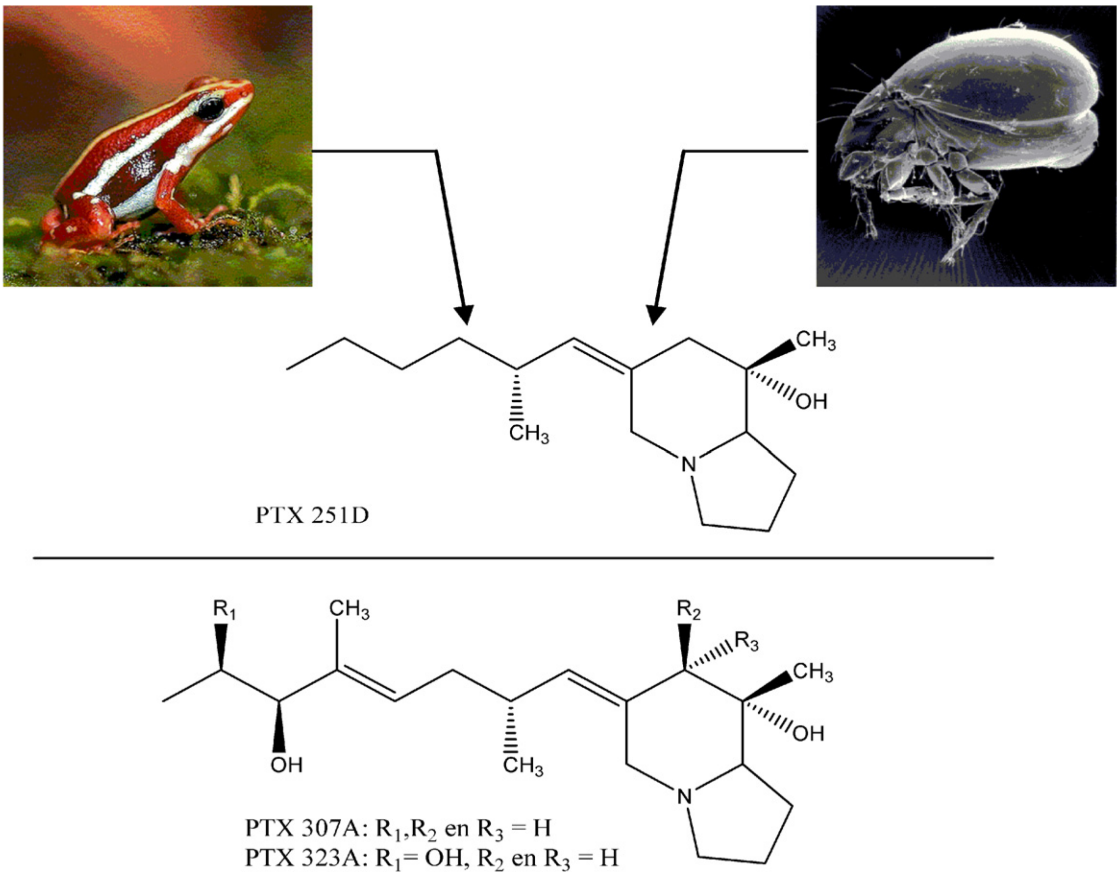


Fig. 1. Structure of PTX **251D**, a lipophilic alkaloid isolated from the skin of some anurans (left *Epipedobates tricolor*) and from Scheloribatid mites (right). Below, structures of related pumiliotoxines PTX **A** (307A) and **B** (323A).

Complex multicellular organisms require rapid and accurate transmission of information among cells and tissues, and tight coordination of distant functions. In both vertebrates and invertebrates, electrical signals control a wide range of physiological processes. All of these processes are mediated in part by members of the voltage-gated ion channel protein superfamily (Yu et al., 2005). VGSCs are transmembrane proteins responsible for action potential initiation and propagation in excitable cells, including nerve, muscle and neuroendocrine cell types. The VGSC consists of a pore-forming $\alpha$-subunit associated with auxiliary $\beta$-subunits. The central, pore-forming $\alpha$-subunit consists of four homologous domains each of which contains six transmembrane $\alpha$-helices. Although sodium channels have broadly similar functional characteristics, small differences in properties do distinguish different isoforms and contribute to their specialized functional roles in mammalian and insect physiology and pharmacology. Until now nine mammalian ($Na_v1.1$–$Na_v1.9$) and three insect VGSCs have been cloned (Yu and Catterall, 2003; Yu et al., 2005). In excitable cells, voltage-gated potassium channels (VGPCs) oppose the action of VGSCs and mediate in this way the repolarization phase and firing frequency of the action potential. VGPCs are also found in non-excitable cells like T-lymphocytes where they participate in the immune response ($K_v1.3$) (Chandy et al., 2004). In contrast to VGSC, a typical VGPC consists of four separate $\alpha$-subunits each containing six transmembrane $\alpha$-helices. The first cloned VGPC was the *Drosophila* voltage-gated *Shaker* channel, and this was rapidly followed by the identification of other VGPC in both insects and mammals. The VGPC superfamily can be divided into up to 12 families with different subunits distinguished again by their contribution in specialized functional roles in physiology and pharmacology (Gutman et al., 2005; Yu et al., 2005).

Since PTX **251D** does not share the known characteristic of PTXs to positively modulate VGSCs, but is able to provoke convulsions and death in both mammalians and insects, we searched in this study for a possible physiological target of PTX **251D**. Given the crucial role that VGSCs and VGPCs play in the central and peripheral nervous system, it is not surprising that a number of venoms from poison dart frogs, scorpions, snakes, etc. target these channels. Therefore, for the very first time, an electrophysiological approach was used to test the synthetic PTX **251D** on an extensive set of VGSCs and VGPCs expressed heterologously in the *Xenopus laevis* oocyte expression system.

## 2. Materials and methods

### 2.1. Toxin

Synthetic (+)-PTX **251D** was kindly provided by Prof. U. Nubbemeyer. The synthetic toxin was found to be identical to the natural occurring (+)-PTX **251D**, based on X-ray analysis (Sudau et al., 2002a, b).

### 2.2. Heterologous expression of voltage-gated ion channels in Xenopus laevis oocytes

For *in vitro* transcription of the tested VGSCs, the following $\alpha$-subunits and $\beta_1$-subunits were, respectively, linearized: $hNa_v1.5$/pSP64T with *Xba*I and $r\beta_1$/pSP64T with *Eco*RI. Capped cRNAs were synthesized from the linearized plasmid using the SP6 mMESSAGE mMACHINE transcription kit (Ambion, USA). The $rNa_v1.2$/pLCT1, $h\beta_1$/pGEM-HE vector, $rNa_v1.4$/pUI-2 vector, *Para*/pGH19-13-5 vector and *tipE*/pGH19 vector were linearized with, respectively, *Not*I and *Nhe*I ($h\beta_1$) and transcribed with the T7 mMESSAGE mMACHINE kit (Ambion, USA).

For *in vitro* transcription of the tested VGPCs, the following $\alpha$-subunits were linearized, respectively, with the corresponding restriction endonucleases: the $rK_v1.1$/pGEM-HE, $rK_v1.2$/pGEM-HE, $hK_v1.3$/pGEM-HE, hERG/pGEM-HE and the *Shaker IR* (inactivation removed)/pGEM-HE vector with *Pst*I, *Sph*I, *Not*I, *Eco*RI and *Nhe*I. The cRNAs were synthesized from the linearized plasmids using the SP6 mMESSAGE mMACHINE transcription kit for hERG and the T7 mMESSAGE mMACHINE transcription kit for $rK_v1.1$, $rK_v1.2$, $hK_v1.3$ and *Shaker IR*.

The harvesting of oocytes from anesthetized female *X. laevis* frogs was as previously described (Abdel-Mottaleb et al. 2006). Oocytes were injected with 50 nl of cRNA at a concentration of $1\,ng\,nl^{-1}$ using a Drummond micro-injector (USA). The solution used for incubating the oocytes contained (in mM): NaCl 96, KCl 2, $CaCl_2$ 1.8, $MgCl_2$ 2 and HEPES 5 (pH 7.4), called ND96 solution, supplemented with $50\,mg\,l^{-1}$ gentamycin sulfate. For expressing of the VGSCs $180\,mg\,l^{-1}$ theophyllin was added in addition to the incubation solution.

### 2.3. Electrophysiological studies on cloned voltage-gated ion channels

Two-electrode voltage-clamp recordings were performed at room temperature (18–22 °C) using a GeneClamp 500 amplifier controlled by a pClamp data acquisition system (Molecular Devices, Axon instruments, USA). Whole-cell currents from *Xenopus* oocytes were recorded 2–4 days after injection. Current and voltage electrodes had resistances as low as possible (0.2–1 MΩ) and were filled with 3 M KCl. Sodium currents were sampled at 5 kHz and filtered at 1 kHz using a four-pole low-pass Bessel filter. Potassium currents were sampled at 500, 250 and 1 kHz and filtered at 200, 100 and 500 Hz for $K_v1.1$–$K_v1.3$, hERG and *Shaker IR*, respectively. Leak subtraction was performed using a $-P/4$ protocol. To eliminate the effect of the voltage drop across the bath-grounding electrode, the bath potential was actively controlled. Voltage records were carefully monitored on an oscilloscope (Hameg). The bath solution was ND96 solution for all VGPCs measured. The VGSCs were measured in ND96 gluconate, ND96 with 96 mM Na-gluconate instead of 96 mM NaCl, in order to reduce endogenous outward $Cl^-$ currents.

Data were analyzed in pClamp8 (Molecular Devices, USA), Winascd (Guy Droogmans, KU-Leuven, Belgium) and in Origin (MicroCal Software, Inc.).

Normalized steady-state activation and inactivation curves were fit with a Boltzmann relationship of, respectively, the form (1) or 1–(1)

$$\frac{1}{1+e^{[(V-V_{1/2})/s]}}, \quad (1)$$

where $V_{1/2}$ is the voltage for half maximal activation or inactivation and $s$ is the slope factor.

In order to determine if the shifts in steady-state activation and inactivation curves were significantly different, an unpaired $t$-test (GraphPad Software, Inc.) was used over a 95% confidence interval.

Changes in the membrane permeability ($P$) ratios of $Na^+$ and $K^+$ were calculated using the Goldman–Hodgkin–Katz (GHK) equation

$$E_{rev} = \left(\frac{RT}{zF}\right) \times \ln\left(\frac{P_{Na} \times [Na]_o + P_K \times [K]_o}{P_{Na} \times [Na]_i + P_K \times [K]_i}\right), \quad (2)$$

where $E_{rev}$ is the reversal potential, $R$ the gas constant, $T$ the absolute temperature (293 K), $z$ the valence ( = 1), $F$ the Faraday's constant, $[Na]_o$ and $[K]_o$ the concentrations of $Na^+$ and $K^+$ outside the oocyte (ND96 solution) and $[Na]_i$ and $[K]_i$ the concentrations of $Na^+$ and $K^+$ inside the oocytes (Weber, 1999).

The ratio $I_{peak\,toxin}/I_{peak\,control}$ was used as a measure for the decrease in peak current induced by the toxin. For $hK_v1.3$ a dose–response curve was constructed, using

$$\%\ \text{inhibition} = \frac{100}{1+(IC_{50}/C)^p}, \quad (3)$$

where $C$ is the toxin concentration, $p$ the Hill coefficient and $IC_{50}$ the toxin concentration needed for half-maximal block.

The voltage dependence of block was fitted with the Woodhull equation (Woodhull, 1973)

$$\frac{I_{PTX\mathbf{251D}}}{I_{control}} = \frac{1}{1+[PTX\mathbf{251D}]/K_d \times e^{-z\delta FV/RT}}, \quad (4)$$

where $I_{PTX\mathbf{251D}}/I_{control}$ is the remaining fraction of the current in the presence of PTX **251D**, [PTX **251D**] the concentration of PTX **251D** (100 μM), $K_d$ is the apparent dissociation constant for PTX **251D** ($10.8 \pm 0.5$ μM at 10 mV), $\delta$ the effective electrical distance and $V$ the test potential. All other parameters have the same meanings as in Eq. (2).

Fig. 2. Panels A–C display a current trace in control conditions (solid line) and in the presence of 100 μM PTX **251D** (dotted line). Representative $Na^+$ currents through $rNa_v1.2/\beta1$, $rNa_v1.4/\beta1$ and $hNa_v1.5/\beta1$, respectively, were obtained by use of the protocols like mentioned on the figures. The time interval between the given pulses was 3 s. Panels E–G show the steady-state activation and inactivation curves of each VGSC in the absence and presence of 100 μM PTX **251D**. The steady-state activation curves were obtained by depolarizing the channels during 50 ms between two potentials (e.g. −70 to +60 mV) starting from a holding potential (e.g. −90 mV). Voltage-dependent steady-state inactivation was determined by means of a double-pulse protocol in which a conditioning pulse was applied from a holding potential of −90 mV to a range of potentials from −85 mV to $V_{max}$, in 5 mV increments for 50 ms immediately followed by a test pulse to $V_{max}$. The time between the given pulses was 3 s for both the activation and inactivation. The peak current amplitudes during the tests were normalized to the amplitude of the first pulse and plotted against the potential of the conditioning pulse. The voltage dependence of relative current (activation and fast inactivation) was fit by a Boltzmann function.

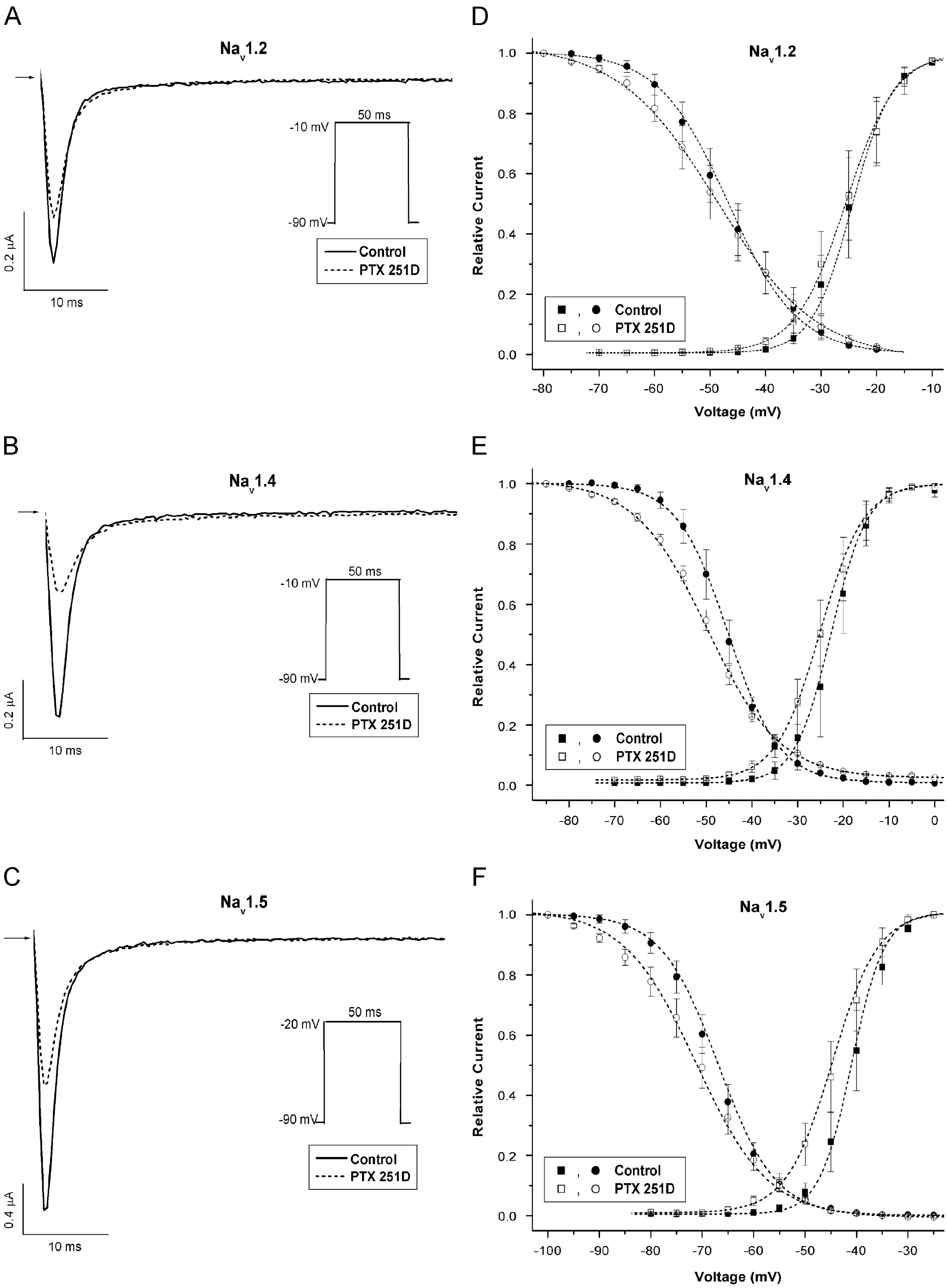
A
Nav1.2
50 ms
-10 mV
-90 mV
Control
PTX 251D
0.2 µA
10 ms
B
Nav1.4
50 ms
-10 mV
-90 mV
Control
PTX 251D
0.2 µA
10 ms
C
Nav1.5
50 ms
-20 mV
-90 mV
Control
PTX 251D
0.4 µA
10 ms
D
Nav1.2
Relative Current
Voltage (mV)
Control
PTX 251D
E
Nav1.4
Relative Current
Voltage (mV)
Control
PTX 251D
F
Nav1.5
Relative Current
Voltage (mV)
Control
PTX 251D

## 3. Results

### 3.1. Effects of PTX **251D** on voltage-gated sodium channels

At a concentration of 100 μM PTX **251D** was able to inhibit all three mammalian VGSCs tested. The percentages of blocks were 29.03±4.83% ($n = 3$), 60.45±4.52% ($n = 3$) and 49.90±2.07% ($n = 8$) for, respectively, $rNa_v1.2/\beta_1$, $rNa_v1.4/\beta_1$ and $hNa_v1.5/\beta_1$ (Fig. 2A–C).

PTX **251D** was also able to shift the $V_{1/2}$, the potential at which the sodium open probability is half maximal, of both the steady-state activation and inactivation curves of each mammalian VGSCs to more negative potentials ($p$-value $<0.05$) (Fig. 2D–F). Table 1 gives an overview of the results of the unpaired $t$-test.

On the insect VGSC *Para/tipE*, 100 μM PTX **251D** shifted the $V_{1/2}$ of the steady-state activation and inactivation curve to more negative potentials ($p$-value $<0.05$) (Table 1). Furthermore, it inhibited dramatically the inactivation of the channel (Fig. 3A–C).

Additionally, 100 μM PTX **251D** changed the ion selectivity of all four VGSCs and thereby shifted the reversal potential ($E_{rev}$) towards more hyperpolarizing potentials. For $rNa_v1.2$, $rNa_v1.4$, $hNa_v1.5$ and *Para/tipE* the shift in $E_{rev}$ was, respectively, 22.0±1.5 mV ($n = 4$); 13.3±4.0 mV ($n = 4$); 29.5±1.8 mV ($n = 3$) and 23.3±4.7 mV ($n = 3$). Fig. 4 shows the shift in $E_{rev}$ for $hNa_v1.5/\beta_1$. From this shift an estimate of the change in ion selectivity in terms of $P_{Na}/P_K$, is calculated using the GHK equation (Eq. (2)). In control conditions the $P_{Na}/P_K$ value is 11.62 indicating an ion permeability ratio ($Na^+$:$K^+$) of 1.00/0.086. These values are in agreement with previously reported ratios (Hille, 1972). After application of 100 μM PTX **251D**, the $P_{Na}/P_K$ value changed to 1.96 leading to a ion permeability ratio of 1.00:0.51. Hence, the presence of the toxin results in a six time higher permeability of the VGSCs for $K^+$ ions.

### 3.2. Effects of PTX **251D** on voltage-gated potassium channels

Based on the symptoms of PTX **251D** in both mammals and insects (*vide supra*) (Bargar et al., 1995; Daly et al., 2003), the toxin was also tested on the mammalian VGPCs $rK_v1.1$, $rK_v1.2$, $hK_v1.3$ and hERG and the insect VGPC *Shaker IR*.

Hundred micromoles of the toxin inhibited the currents of *Shaker IR* channels with 2.70±0.96% ($n = 3$), hERG with 18.75±7.73 ($n = 4$), $rK_v1.1$ with 40.35±4.37% ($n = 3$), $rK_v1.2$ with 11.01±1.55% ($n = 3$) and $hK_v1.3$ with 90.35±3.32% ($n = 6$) (Fig. 5A–E). For $hK_v1.3$, which was the most sensitive channel, a dose–response curve was constructed (Fig. 5H). The $IC_{50}$ value was 10.8±0.5 μM with a Hill-coefficient value of 1. Fig. 5F shows the normalized $I$–$V$ relation of $hK_v1.3$ in absence and presence of 100 μM PTX **251D**. The shift in $V_{1/2}$ to more negative potentials was not significant ($p$-value = 0.1533) (Table 1). Voltage dependence of block was measured by fitting fractional unblock as a function of the voltage with the Woodhull equation (Eq. (4)). The effective electrical distance $\delta$ obtained from fitting of block at 100 μM PTX **251D** was 0.56±0.08 ($n = 4$).

In addition, PTX **251D** had an effect on the deactivation kinetics of the potassium channel $rK_v1.1$–1.2, $hK_v1.3$ and *Shaker IR* (Fig. 5A, C and D).

Table 1

Summary of $V_{1/2}$±SEM and $p$-values of the steady-state activation and inactivation curves from all tested VGSCs and from VGPC $hK_v1.3$ in both control conditions and after application of 100 μM PTX **251D**

| | Steady-state activation curve | | | Steady-state inactivation curve | | |
|---|---|---|---|---|---|---|
| | Mean $V_{1/2}$±SEM in control conditions (mV) | Mean $V_{1/2}$±SEM after 100 μM PTX **251D** (mV) | $p$-value | Mean $V_{1/2}$±SEM in control conditions (mV) | Mean $V_{1/2}$±SEM after 100 μM PTX **251D** (mV) | $p$-value |
| $rNa_v1.2/\beta1$ ($n = 4$) | −24.4±0.3 | −25.5±0.3 | 0.0206 | −46.7±0.3 | −48.7±0.7 | 0.0021 |
| $rNa_v1.4/\beta1$ ($n = 4$) | −22.7±0.4 | −25.1±0.4 | 0.0027 | −45.2±0.2 | −49.7±0.2 | <0.0001 |
| $hNa_v1.5/\beta1$ ($n = 3$) | −40.9±0.4 | −44.7±0.5 | 0.0020 | −66.9±0.4 | −71.2±0.8 | 0.0043 |
| Para/tipE ($n = 3$) | −20.8±0.2 | −33.8±0.2 | <0.0001 | −43.64±0.23 | −49.38±0.73 | 0.0017 |
| $hK_v1.3$ ($n = 4$) | −27.6±0.7 | −27.1±0.7 | 0.4499 | | | |

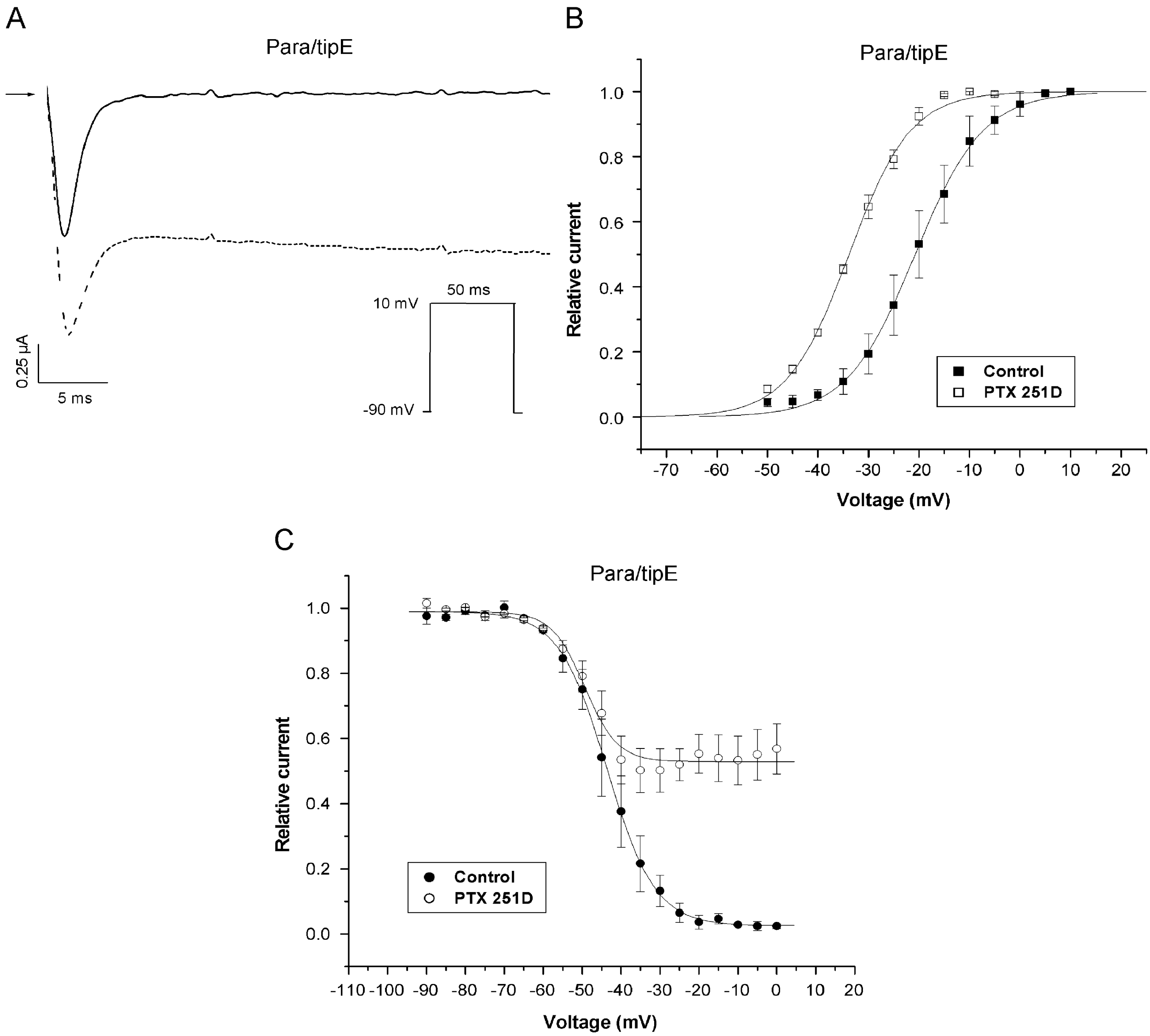


Fig. 3. Panel (A) displays a $Na^+$ current trace of *Para/tipE* in control conditions (solid line) and in the presence of 100 μM PTX **251D** (dotted line). Representative $Na^+$ currents were obtained by use of the protocols like mentioned in the figures. The time interval between the given pulses was 3 s. Panels (B) and (C) show, respectively, the steady-state activation and inactivation curves of *Para/tipE* in the absence and presence of 100 μM PTX **251D**. Both curves were obtained as mentioned in the legend of Fig. 2.

## 4. Discussion

PTXs play a major role in the chemical defense of certain anurans and possibly have an identical function in some arthropods (Daly et al., 2003; Weldon et al., 2006). They are very toxic and known for their strong cardiotonic activity, which is dependent on the structure of the side chain. PTX **B** (323A) (Fig. 1), which has two hydroxyl groups in the side chain, had both positive ionotropic and chronotropic effects on spontaneously beating guinea pig atrial strips. PTX **A** (307A) (Fig. 1), which lacks the 7′-hydroxyl group present in the side chain of PTX **B**, caused a lower increase in force of contracture while having minimal effects on the frequency. The positive effects of PTXs such as PTX **B** and **A** are due to an inhibition of the inactivation of VGSCs, resulting in the breakdown of phosphoinositides and the release of stored $Ca^{2+}$ ions (Daly et al., 1990). In contrast, PTX **251D** (Fig. 1), which only differs from PTX **A** and PTX **B** in having a simple methylhexylidene side chain,

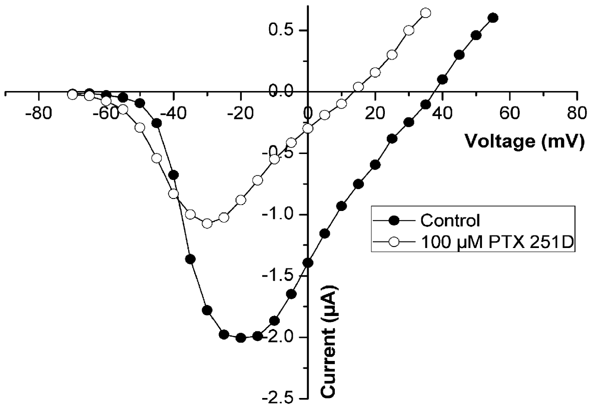


Fig. 4. *I–V* curve from heart muscle VGSC hNa$_v$1.5/β1 in the absence and presence of 100 μM PTX **251D**. The *I–V* curve was obtained by depolarizing the channels during 50 ms between −70 and +65 mV starting from a holding potential of −90 mV. The time between the given pulses was 3 s.

acted as a cardiac depressor (Daly et al., 1985, 1988).

The results presented in this work show that 100 μM of PTX **251D** inhibited the mammalian VGSCs rNa$_v$1.2/β1, rNa$_v$1.4/β1 and hNa$_v$1.5/β1 in a dose-dependent way in the concentration range from 1 to 100 μM. A stimulatory effect at low concentrations (10 μM) as mentioned in previous studies (Daly et al., 1990) has not been observed in the *Xenopus* oocyte expression system. The effect on the cardiac VGSC hNa$_v$1.5/β1 might explain the action of the PTX **251D** as cardiac depressor (Daly et al., 1985). Additionally, the toxin shifts both the steady-state activation and inactivation curves to more negative potentials. Comparison between the panels 2A–C and 2D–F shows that there is no statistical difference in shift in the steady-state inactivation curves of the three mammalian VGSCs at potentials where the $Na^+$ current was maximally inhibited. This means that the inhibition cannot be explained by the shift in the steady-state inactivation curves, but possibly through an apparent pore-blocking mechanism, which could be linked to the altered ion selectivity associated with a reduction of the driving force of the current (Fig. 4).

Interestingly, 100 μM PTX **251D** shifts not only the steady-state inactivation curve of the insect VGSC *Para/tipE* to more negative values and the steady-state activation curve to even more negative potentials compared to the shifts in steady-state activation curves of the mammalian VGSCs, it also dramatically inhibits its inactivation. Inhibition of the inactivation together with a shift from the activation towards hyperpolarizing potentials is a common characteristic of lipid-soluble neurotoxins binding to receptor site-2 (Wang and Wang, 2003; Tikhonov and Zhorov, 2005). Another common characteristic of such toxins is the loss of the strong selectivity towards $Na^+$ ions as well as the use-dependent action (e.g. batrachotoxin, veratridine and aconitine). Although PTX **251D** does not act in a use-dependent way (data not shown), it modulates the VGSC *Para/tipE* in a similar way like diverse lipid-soluble activators. However, the only shared characteristics on the mammalian VGSCs are the change in ion selectivity and the hyperpolarizing shift in the activation process.

In addition to the modulation of VGSCs, PTX **251D** also modulated VGPCs with hK$_v$1.3 being the most sensitive ($IC_{50} = 10.8\,\mu M$). To the best of our knowledge, this is the first report of a lipophilic alkaloid isolated from anuran skin that modulates VGPCs (Daly et al., 2005). The molecular mechanism of block, however, remains to be elucidated. Since at physiological pH the tertiary amine function of the indolizidin ring will be partially protonated, it could be that PTX **251D** blocks potassium channels in the same way alkyl TEA molecules do (Kimbrough and Gingrich, 2000; Hille, 2001a, b). The TEA receptor of *Shaker* VGPCs is located in the S6 segments (Yellen, 1998) and it is proved that the alkyl tail (C>6) of alkyl TEA molecules interacts with a hydrophobic-binding pocket located in the S6 segments (Choi et al., 1993; Kimbrough and Gingrich, 2000). Due to the voltage dependency of PTX **251D** (Fig. 5G), it is possible that the charged amine group of the toxin is pushed more into the pore vestibule during more positive potentials, resulting in a higher block. Out of the calculated electrical distance (0.56 ± 0.08) we can assume that the positively charged PTX **251D** senses 60% of the membrane electrical field.

Together with the block, a dramatical slowing of tail currents is noticed. PTX **251D** probably increases the time constant of deactivation, which, together with the reduction of peak current, results in a crossing from the tail currents. Since it has been hypothesized that the activation gate is located at the cytoplasmic end of the S6 segments (del Camino and Yellen, 2001), a possible explanation for this phenomenon is that the toxin binds to the S6 segments and immobilizes them. Such immobilization could "freeze" the channel in the open state, causing a change in conformation that prevents the channel from closing. If so, this theory supports

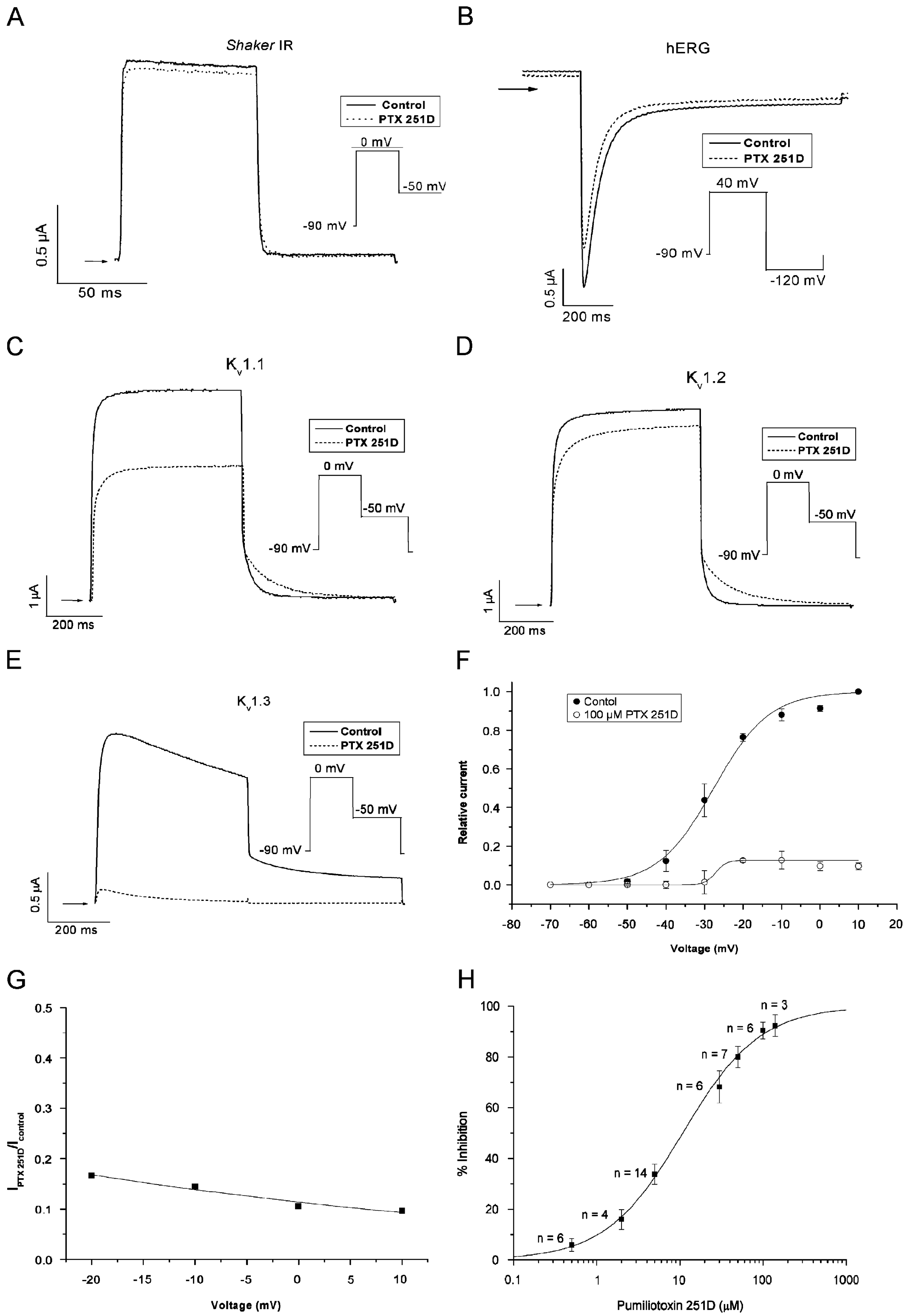


Fig. 5. Panels (A–E) display a $K^+$ current trace in control conditions (solid line) and in presence of 100 μM PTX **251D** (dotted line). Representative $K^+$ currents were obtained by use of the protocols mentioned in the figures. The time interval between the pulses was 5 s. Panel (F) shows the normalized *I–V* curve from $hK_v1.3$ in absence and presence of 100 μM PTX **251D**. The curve was obtained by depolarizing the channels during 500 ms between −70 and +10 mV starting from a holding potential of −90 mV. The time between the given pulses was 5 s. In panel (G) the $I_{PTX251D}/I_{control}$ is plotted against the voltage (potentials −50 and −40 mV or not shown because of the threshold of activation) in order to demonstrate the voltage dependence of PTX **251D** block. Panel (H) shows the dose–response curve for $hK_v1.3$. The IC50 value was $10.8 \pm 0.5$ μM.

again the importance of the S6 segments as part of the binding site for PTX **251D**. Mutagenesis studies will need to be performed to explain why $hK_v1.3$ is the most sensitive channel.

Earlier studies on mice have shown that a subcutaneous injection of 10 mg/kg induces an apparent marked pain at the injection site and hyperactivity. In 1 min, running convulsions commenced, leading to death after several minutes (Daly et al., 2003). If a plasma volume of 78 ml/kg is taken into account, it is reasonable to assume that the free plasma level of PTX **251D** should reach 100 μM in the tested mice. Although nothing is known of how well PTX **251D** penetrates into the brain where convulsions are probably elicited, the observation of convulsions can be explained through inhibition of VGPCs. Initial experiments with anticonvulsants showed that the toxic effects of PTX **251D** can be reduced by carbamazepine targeting $Na^+$ channels and phenobarbital targetting $GABA_A$ receptors and $Ca^{2+}$ channels, whereas diazepam and dizocilpine targeting, respectively, $GABA_A$ and NMDA receptors were ineffective (McNamara, 1995). A similar pharmacological study has been done on the ability of anticonvulsant drugs to protect against 4-aminopyridine-induced convulsions (Yamaguchi and Rogawski, 1992).

The $K^+$ channel blocker 4-aminopyridine is a potent convulsant in animals and man. In mice, a subcutaneous injection of 13.3 mg/kg 4-aminopyridine produces behavioral activation, clonic limb movements and wild running, followed by tonic hindlimb extension and death. These toxic effects could also be reduced by carbamazepine and phenobarbital but not by diazepam and dizocilpine.

The results obtained with PTX **251D** on VGSCs and VGPCs make this toxin and PTX homologues in general an attractive tool for further study. It is fascinating that one molecule both inhibits VGSCs and VGPCs and in addition modulates mammalian and insect ion channels in a different way. Through mutagenesis studies and patch-clamp experiments, it would be interesting to explore the receptor site of PTX **251D** and characterize the electrophysiological behavior of the toxin in detail.

Considered the many functions of $hK_v1.3$, from regulation of neuronal stability to its role in immunity, metabolism, insulin resistance, sensory discrimination and axonal targeting (Cahalan et al., 2001; Xu et al., 2003, 2004; Chandy et al., 2004; Fadool et al., 2004), derivatives of PTX **251D** can act as potential non-peptide candidates for medicines targeting diseases related to $hK_v1.3$. Together with its recently discovered role as an insect repellent (Weldon et al., 2006), the effects described in this paper on the insect VGSC *Para/tipE*, make PTX **251D** and its derivatives interesting candidates for developing insecticides.

## Acknowledgments

We would like to thank the following persons: S.C. Cannon, University of Texas Southwestern Medical Center, Dallas, USA, for sharing the hβ1 subunit, A.L. Goldin, University of California, Irvine, USA, for sharing $Na_v1.2$, G. Mandel, State University of New York, USA, for sharing $Na_v1.4$; R.G. Kallen, University of Pennsylvania, Philadelphia, USA, for sharing $Na_v1.5$, Martin S. Williamson, IACR-Rothamsted, UK for sharing the para and tipE clone, S.H. Heinemann, Friedrich-Schiller-Universität Jena, Germany for sharing the $r\beta_1$ subunit, G. Yellen, Harvard University, Boston, USA, for sharing the *Shaker IR*, Olaf Pongs, Universitaet Hamburg, Hamburg, Germany, for providing the cDNA for the $K_v1.2$ channel and Maria L. Garcia, Merck Research Laboratories, USA, for $K_v1.3$. Finally, we thank Sarah Debaveye for technical assistance and Dr. Elke Vermassen for critical remarks.

T.V. and C.M. are respectively research assistant (aspirant) and postdoctoral research fellow (postdoctoraal onderzoeker) of the Fund for Scientific Research—Flanders (F.W.O.-Vlaanderen). Y.A. is a doctoral student supported by IRO KULeuven scholarship. This work was supported by the following grants: G.0330.06 (F.W.O.-Vlaanderen), OT-05-64 (K.U.Leuven) and P6/31 (Interuniversity Attraction Poles Programme—Belgian State—Belgian Science Policy).

## References

Abdel-Mottaleb, Y., Coronas, F.V., de Roodt, A.R., Possani, L.D., Tytgat, J., 2006. A novel toxin from the venom of the scorpion *Tityus trivittatus*, is the first member of a new alpha-KTX subfamily. FEBS Lett. 580, 592–596.

Bargar, T.M., Lett, R.M., Johnson, P.L., Hunter, J.E., Chang, C.P., Pernich, D.J., Sabol, M.R., Dick, M.R., 1995. Toxicity of pumiliotoxin 251D and synthetic analogs to the cotton pest *Heliothis virescens*. J. Agric. Food Chem. 43, 1044–1051.

Cahalan, M.D., Wulff, H., Chandy, K.G., 2001. Molecular properties and physiological roles of ion channels in the immune system. J. Clin. Immunol. 21, 235–252.

Chandy, K.G., Wulff, D., Beeton, D., Pennington, M., Gutman, G.A., Cahalan, M.D., 2004. K+ channels as targets for specific immunomodulation. Trends Pharmacol. Sci. 25, 280–289.

Choi, K.L., Mossman, C., Aube, J., Yellen, G., 1993. The internal quaternary ammonium receptor site of Shaker potassium channels. Neuron 10, 533–541.

Daly, J.W., McNeal, E.T., Overman, L.E., Ellison, D.H., 1985. A new class of cardiotonic agents: structure–activity correlations for natural and synthetic analogues of the alkaloid A new class of A new class of cardiotonic agents: structure–activity correlations for natural and synthetic analogues of the alkaloid pumiliotoxin B (8-hydroxy-8-methyl-6-alkylidene-1-azabicyclo[4.3.0]nonanes). J. Med. Chem. 28, 482–486.

Daly, J.W., McNeal, E., Gusovsky, F., Ito, F., Overman, L.E., 1988. Pumiliotoxin alkaloids: relationship of cardiotonic activity to sodium channel activity and phosphatidylinositol turnover. J. Med. Chem. 31, 477–480.

Daly, J.W., Gusovsky, F., McNeal, E.T., Secunda, S., Bell, M., Creveling, C.R., Nishizawa, Y., Overman, L.E., Sharp, M.J., Rossignol, D.P., 1990. Pumiliotoxin alkaloids: a new class of sodium channel agents. Biochem. Pharmacol. 40, 315–326.

Daly, J.W., Garraffo, H.M., Spande, T.F., Clark, V.C., Ma, J., Ziffer, H., Cover Jr., J.F., 2003. Evidence for an enantioselective pumiliotoxin 7-hydroxylase in dendrobatid poison frogs of the genus Dendrobates. Proc. Natl. Acad. Sci. USA 100, 11092–11097.

Daly, J.W., Spande, T.F., Garraffo, H.M., 2005. Alkaloids from amphibian skin: a tabulation of over eight-hundred compounds. J. Nat. Prod. 68, 1556–1575.

del Camino, D., Yellen, G., 2001. Tight steric closure at the intracellular activation gate of a voltage-gated K(+) channel. Neuron 32, 649–656.

Fadool, D.A., Tucker, K., Perkins, R., Fasciani, G., Thompson, R.N., Parsons, A.D., Overton, J.M., Koni, P.A., Flavell, R.A., Kaczmarek, L.K., 2004. Kv1.3 channel gene-targeted deletion produces "Super-Smeller Mice" with altered glomeruli, interacting scaffolding proteins, and biophysics. Neuron 41, 389–404.

Gutman, G.A., Chandy, K.G., Grissmer, S., Lazdunski, M., McKinnon, D., Pardo, L.A., Robertson, G.A., Rudy, B., Sanguinetti, M.C., Stuhmer, W., Wang, X., 2005. International Union of Pharmacology LIII. Nomenclature and molecular relationships of voltage-gated potassium channels. Pharmacol. Rev. 57, 473–508.

Hille, B., 1972. The permeability of the sodium channel to metal cations in myelinated nerve. J. Gen. Physiol. 59, 637–658.

Hille, B., 2001a. Ion Channels of Excitable Membranes. Sinauer Associates, Inc., Sunderland, MA, USA, pp. 63–65, 69.

Hille, B., 2001b. Ion Channels of Excitable Membranes. Sinauer Associates, Inc., Sunderland, MA, USA, pp. 511–516.

Kimbrough, J.T., Gingrich, K.J., 2000. Quaternary ammonium block of mutant Na+ channels lacking inactivation: features of a transition-intermediate mechanism. J. Physiol. 529 (Pt 1), 93–106.

McNamara, J.O., 1995. In: Hardman, J.G., Gilman, A.G., Limbird, L.E. (Eds.), Goodman and Gilman's The Pharmacological Basis of Therapeutics. McGraw-Hill, New York, pp. 461–486.

Saporito, R.A., Garraffo, H.M., Donnelly, M.A., Edwards, A.L., Longino, J.T., Daly, J.W., 2004. Formicine ants: an arthropod source for the pumiliotoxin alkaloids of dendrobatid poison frogs. Proc. Natl. Acad. Sci. USA 101, 8045–8050.

Saporito, R.A., Donnelly, M.A., Norton, R.A., Garraffo, H.M., Spande, T.F., Daly, J.W., 2007. Oribatid mites as a major dietary source for alkaloids in poison frogs. Proc. Natl. Acad. Sci. USA 104, 8885–8890.

Sudau, A., Munch, W., Bats, J.W., Nubbemeyer, U., 2002a. Total synthesis of (+)-pumiliotoxin 251D (Part 1): synthesis of the bicyclic core. Eur. J. Org. Chem., 3304–3314.

Sudau, A., Munch, W., Bats, J.W., Nubbemeyer, U., 2002b. Total synthesis of (+)-pumiliotoxin 251D (Part 2): introduction of the side chain. Eur. J. Org. Chem., 3315–3325.

Takada, W., Sakata, T., Shimano, S., Enami, Y., Mori, N., Nishida, R., Kuwahara, Y., 2005. Scheloribatid mites as the source of pumiliotoxins in dendrobatid frogs. J. Chem. Ecol. 31, 2403–2415.

Tikhonov, D.B., Zhorov, B.S., 2005. Sodium channel activators: model of binding inside the pore and a possible mechanism of action. FEBS Lett. 579, 4207–4212.

Wang, S.Y., Wang, G.K., 2003. Voltage-gated sodium channels as primary targets of diverse lipid-soluble neurotoxins. Cell. Signal. 15, 151–159.

Weber, W., 1999. Ion currents of *Xenopus laevis* oocytes: state of the art. Biochim. Biophys. Acta 1421, 213–233.

Weldon, P.J., Kramer, M., Gordon, S., Spande, T.F., Daly, J.W., 2006. A common pumiliotoxin from poison frogs exhibits enantioselective toxicity against mosquitoes. Proc. Natl. Acad. Sci. USA 103, 17818–17821.

Woodhull, A.M., 1973. Ionic blockage of sodium channels in nerve. J. Gen. Physiol. 61, 687–708.

Xu, J., Koni, P.A., Wang, P., Li, G., Kaczmarek, L., Wu, Y., Li, Y., Flavell, R.A., Desir, G.V., 2003. The voltage-gated potassium channel Kv1.3 regulates energy homeostasis and body weight. Hum. Mol. Genet. 12, 551–559.

Xu, J., Wang, P., Li, Y., Li, G., Kaczmarek, L.K., Wu, Y., Koni, P.A., Flavell, R.A., Desir, G.V., 2004. The voltage-gated potassium channel Kv1.3 regulates peripheral insulin sensitivity. Proc. Natl. Acad. Sci. USA 101, 3112–3117.

Yamaguchi, S., Rogawski, M.A., 1992. Effects of anticonvulsant drugs on 4-aminopyridine-induced seizures in mice. Epilepsy Res. 11, 9–16.

Yellen, G., 1998. The moving parts of voltage-gated ion channels. Q. Rev. Biophys. 31, 239–295.

Yu, F.H., Catterall, W.A., 2003. Overview of the voltage-gated sodium channel family. Genome Biol. 4, 207.

Yu, F.H., Yarov-Yarovoy, V., Gutman, G.A., Catterall, W.A., 2005. Overview of molecular relationships in the voltage-gated ion channel superfamily. Pharmacol. Rev. 57, 387–395.